THE JOURNAL OF PHYSICAL CHEMISTRY A

Article

pubs.acs.org/JPCA

Resonance Raman Spectra of TNT and RDX Using Vibronic Theory, Excited-State Gradient, and Complex Polarizability Approximations

W. A. Al-Saidi,*[,†] Sanford A. Asher,[‡] and Patrick Norman[§]

[†]Department of Chemical and Petroleum Engineering, University of Pittsburgh, Pittsburgh, Pennsylvania 15261, United States

[‡]Department of Chemistry, University of Pittsburgh, Pittsburgh, Pennsylvania 15260, United States

[§]Department of Physics, Chemistry and Biology, Linköping University, SE-581 83 Linköping, Sweden

ABSTRACT: Geometries, UV absorption bands, and resonance Raman (RR) cross sections of TNT and RDX are investigated using density functional theory (DFT) in conjunction with the Coulomb attenuated B3LYP exchange-correlation functional. The absorption and RR spectra are determined with use of vibronic (VB) theory, excited-state gradient, and complex polarizability (CPP) approximations. We examined low-energy isomers (two for TNT and four for RDX) whose energies differ by less than 1 kcal/mol, such that they would appreciably be populated at room temperature. The two TNT isomers differ by an internal rotation of the methyl group, while the four conformers of RDX differ by the arrangements of the nitro group relative to the ring. Our theoretical optical properties of the TNT and RDX isomers are in excellent agreement with experimental and recent CCSD-EOM results, respectively. For the two TNT isomers, the ultraviolet RR (UVRR) spectra are similar and in good agreement with recently measured experimental results. Additionally, the UVRR spectra computed using the excited-state and CPP approaches compare favorably with the VB theory results. On the other hand, the RR spectra of the RDX conformers differ from one another, reflecting the importance of the positioning of the NO_2 groups with respect to the ring. In the gas phase or in solution, RDX would give a spectrum associated with a conformationally averaged structure. It is encouraging that the computed spectra of the conformers show similarities to recent measured RDX spectra in acetonitrile solution, and reproduce the 10-fold decrease in the absolute Raman cross sections of RDX compared to TNT for the observed 229 nm excitation. We show that in TNT and RDX vibrational bands that couple to NO_2 or the ring are particularly resonance enhanced. Finally, the computed RDX spectra of the conformers present a benchmark for understanding the RR spectra of the solid-phase polymorphs of RDX.

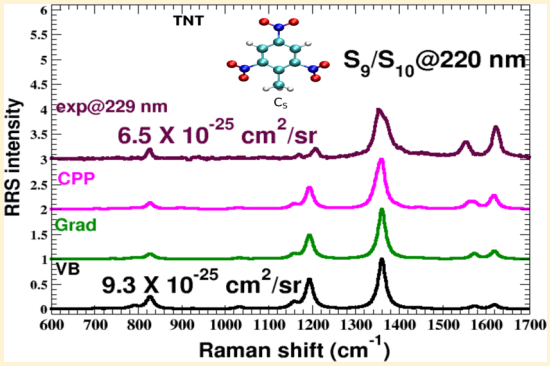

INTRODUCTION

Raman spectroscopy is a form of inelastic light scattering associated with shifts in photon energies due to vibrational energy level changes. Normally, the Raman intensities are weak but selected vibrational modes can be enhanced by several orders of magnitude (10^4–10^6) if the light frequency is tuned into an electronic absorption band. Resonance Raman (RR) spectroscopy is a versatile tool that finds applications in many different fields,[1,2] ranging from small molecules to complex biological systems.[3,4] The ultrahigh sensitivity and selectivity of RR enables the detection of minute amounts of substances, such as explosives.[5,6] RR spectroscopy is also one of the rare experimental tools in physical chemistry that probes excited-state potential energy surfaces, and, from a theoretical perspective, it provides a means to benchmark theoretical ground- and excited-state models.

The theory of Raman scattering from isolated molecules is well established by Kramers and Heisenberg[7] and independently by Dirac.[8] The Kramers–Heisenberg–Dirac (KHD) theory is the starting point for all theoretical work of Raman scattering, where the Raman polarizability that contributes to the transition between molecular states $|i\rangle$ and $|f\rangle$ is written as a sum-over-states expression including all rovibronic states of the molecule.

The VB theory by Albrecht and co-workers represents a modern formulation of the theory for RR scattering.[9,10] It is based on the Born–Oppenheimer approximation to achieve a decoupling of the electronic and nuclear degrees of freedom, so that a VB state can be expanded into products of electronic and vibrational states. Expanding the transition dipole moment in terms of normal coordinates of the ground state, the Albrecht *A*- and *B*-scattering terms can be identified. The *A*-term describes the Franck–Condon contribution and the *B*-term describes Herzberg–Teller type activities. The *A*-term typically dominates for strong electronic resonances. Due to the summations over all vibrational states, the VB theory becomes quite computationally intractable for large systems. Most calculations adopting it are based on two alternative approaches: (i) the time-dependent wave packet theory[11−13] or (ii) the transform theory.[14] In both cases, the daunting

Received: April 23, 2012
Revised: June 30, 2012
Published: July 8, 2012

vibrational state summation is avoided at the expense of introducing additional approximations.

The transform theory establishes a relation between the optical absorption and the polarizability, as these are connected by the Kramers−Kronig relation. The optical absorption can be measured and used to compute the polarizability, thereby circumventing the cumbersome sum over states in the VB theory. In practical applications, the following assumptions are also made in transform theory: (i) ground- and excited-state potentials are harmonic, (ii) non-Condon effects are negligible, (iii) the temperature is low enough to restrict all transitions to originate from the ground vibrational state, (iv) vibrational frequencies of the ground and excited states are identical, and (v) only one excited electronic state is important. Recently, Guthmuller and Champagne applied transform theory but avoided the use of experimental input and instead calculated the Raman tensor by evaluating the sum-over-vibrational-states using quantum chemical approaches.[15−17]

If the long-time nuclear dynamics can be neglected, the vibronic theory can be further simplified so that the RR polarizability tensor is obtained from the changes of the electronic polarizability with respect to nuclear motion as adopted in nonresonant, or normal, Raman scattering. There is no resolution made of individual vibrational levels in the excited states and all mechanisms of broadening of absorption bands are combined into a single phenomenological relaxation, or damping parameter. This makes the approach useful for medium- and large-scale systems at room temperature, where broad structureless UV-absorption bands occur. On the other hand, there is no truncation made in the summation over electronic states, meaning that a full coupling of absorption bands is retrieved in the calculation, that can be important for molecules with a high degree of symmetry and/or high density of states. From these perspectives, the simplifications made in the short-time approximation are quite different from those discussed above. This approach requires the determination of the derivatives of the electronic polarizability with respect to normal-mode displacements at resonance frequencies[18,19] that can be easily accomplished by the use of the complex polarization propagator (CPP) theory.[20]

In this paper, we investigate the RR scattering of 2-methyl-1,3,5-trinitrobenzene (TNT) and 1,3,5-trinitroperhydro-1,3,5-triazine (RDX) in the gas phase. The interest in this study is for both fundamental as well as practical reasons because TNT and RDX are both highly energetic materials. There is a growing interest in the development of new analytical methods for the detection of trace levels of explosives. Deep UVRR spectroscopy is very promising as it can detect explosives at parts-per-billion concentrations. We compare spectra obtained with the VB theory and the short-time approximation. We will compare our results to recent experimental UVRR measurements.[5,6] Both TNT and RDX have multiple conformers (shown schematically in Figure 1) some of which differ by less than 1 kcal/mol. At room temperature, all of these conformers contribute to the gas-phase population. For this reason, we have studied the RR spectra of the lowest two TNT conformers and the lowest four RDX conformers.

THEORETICAL APPROACH

In the standard experimental setup for Raman spectroscopy, the incident light of frequency ω is linearly polarized and detection is made over all scattered polarizations in a direction perpendicular to the direction of propagation as well as

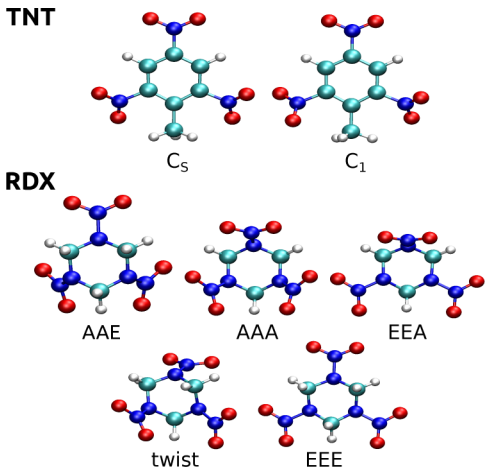

Figure 1. Molecular structures of the TNT and RDX conformers under investigation. Hydrogen, carbon, nitrogen, and oxygen are shown as white, cyan, blue, and red spheres, respectively.

polarization of the incident beam. Each vibrational normal mode ν with frequency ω_ν gives rise to a dipole oscillating at frequency $\omega-\omega_\nu$, with an intensity proportional to the differential Raman cross section:

$$\frac{d\sigma_\nu}{d\Omega} = \frac{1}{16\pi^2\varepsilon_0^2 c^4}\frac{(\omega-\omega_\nu)^4}{1-\exp(-\hbar\omega_\nu/k_B T)} \times S_\nu \quad (1)$$

where T is the temperature and S_ν is the scattering factor, otherwise known as Raman activity that is related to the Raman polarizability tensor $\alpha_{\alpha\beta}^{fi}$ that contributes to a transition between the initial $|i\rangle$ and final $|f\rangle$ molecular states (that is, S_ν is a pure molecular property expressed in terms of tensor averages that depend on the experimental setup).

To write explicitly the dependence of S_ν on $\alpha_{\alpha\beta}^{fi}$, we assume for convenience that the incident beam propagates along the Z-direction and is polarized along the Y-direction, and the scattered beam is detected along the X-direction. Also, to simplify the notation, we use α_{YY}^{fi} instead of $\alpha_{YY}^{fi}(\omega)$, etc., so that S_ν can be written as[19]

$$S_\nu = |\overline{\alpha_{YY}^{fi}\alpha_{YY}^{fi}} + \overline{\alpha_{ZY}^{fi}\alpha_{ZY}^{fi}}| \quad (2)$$

where

$$\overline{\alpha_{YY}^{fi}\alpha_{YY}^{fi}} = \overline{\alpha^{fi}}^2 + \frac{4}{45}\gamma^2 \quad (3)$$

$$\overline{\alpha_{ZY}^{fi}\alpha_{ZY}^{fi}} = \frac{1}{15}\gamma^2 \quad (4)$$

The overbar indicates orientational averaging to account for the randomly oriented molecular configurations, and $\overline{\alpha^{fi}}$ and γ^2 are the Raman invariants of $\alpha_{\alpha\beta}^{fi}$ defined as

$$\overline{\alpha^{fi}} = \frac{1}{3}(\alpha_{xx}^{fi} + \alpha_{yy}^{fi} + \alpha_{zz}^{fi}) \quad (5)$$

$$\gamma^2 = \frac{1}{2}[(\alpha_{xx}^{fi} - \alpha_{yy}^{fi})^2 + (\alpha_{xx}^{fi} - \alpha_{zz}^{fi})^2 + (\alpha_{yy}^{fi} - \alpha_{zz}^{fi})^2 + 6(\alpha_{xy}^{fi}\alpha_{xy}^{fi} + \alpha_{xz}^{fi}\alpha_{xz}^{fi} + \alpha_{yz}^{fi}\alpha_{yz}^{fi})] \quad (6)$$

Thus, the calculation of the normal and resonant Raman cross section follows once $\alpha_{\alpha\beta}^{fi}$ is known. In the case of normal Raman scattering, the polarizability tensor is real, whereas, in the

dx.doi.org/10.1021/jp303920c | J. Phys. Chem. A 2012, 116, 7862−7872

resonant case, it is complex. Below, we summarize briefly the three approaches that we use to compute $\alpha_{\alpha\beta}^{fi}$, or the Raman intensity, based on VB theory, excited-state gradient approximation, and CPP respectively.

In VB theory, using the Peticolas and Rush expressions, the Raman polarizability tensor $\alpha_{\alpha\beta}^{fi}$ is expressed as[14,21]

$$\alpha_{\alpha\beta}^{fi} = \frac{1}{\hbar}\sum_{e} \mu_{\alpha}^{eg}\mu_{\beta}^{eg}\frac{\Delta_{e,\nu}}{\sqrt{2}}[\Phi(\omega) - \Phi(\omega - \omega_{\nu})] \tag{7}$$

where $\boldsymbol{\mu}^{eg}$ is the electronic transition moment between the ground state g and the excited state e, $\Delta_{e,\nu}$ is the dimensionless displacement along the νth normal coordinate between the ground state and excited potential minima, and the sum over excited states e accounts for contributions of multiple excited states. The function $\Phi(\omega)$ is defined as

$$\Phi(\omega) = \sum_{\{u\}} \frac{\Pi_{\nu}|\langle\chi_{g0_{\nu}}|\chi_{eu_{\nu}}\rangle|^2}{\omega_{e,g} + \sum_{\nu} u_{\nu}\omega_{\nu} - \omega - i\Gamma} \tag{8}$$

where the summation over $\{u\}$ includes all of the vibrational quantum numbers of the modes considered, $\omega_{e,g}$ is the 0−0 transition frequency, and Γ is a damping term associated with homogeneous broadening. The Franck−Condon overlap integrals $\langle\chi_{g0_{\nu}}|\chi_{eu_{\nu}}\rangle$ are given analytically in the independent-mode displaced-harmonic oscillator model as

$$|\langle\chi_{g0_{\nu}}|\chi_{eu_{\nu}}\rangle|^2 = \frac{\Delta_{e,\nu}^{2u_{\nu}}}{2^{u_{\nu}}u_{\nu}!}e^{-\Delta_{e,\nu}^2/2} \tag{9}$$

Additionally, the displacements $\Delta_{e,\nu}$ are determined from the partial derivatives of the vertical electronic excitation energies, E_{vert}^{e} along the vibrational normal coordinates Q_{ν} at the ground-state equilibrium position according to[15]

$$\Delta_{e,\nu} = -\frac{1}{\sqrt{\hbar}\,\omega_{\nu}^{3/2}}\left(\frac{\partial E_{\mathrm{vert}}^{e}}{\partial Q_{\nu}}\right)_0 \tag{10}$$

The excited-state gradient approach, which is valid under the short-time approximation, simplifies the VB theory as it relies only on the geometrical displacements $\Delta_{e,\nu}$. In this case

$$S_{\nu} \propto {\omega_{\nu}}^2\Delta_{e,\nu}^2 \tag{11}$$

In the CPP approach,[18,19] which is also valid under the short-time approximation, $\alpha_{\alpha\beta}^{fi}$ is determined in the harmonic approximation as

$$\alpha_{\alpha\beta}^{fi} = \sqrt{\frac{\hbar}{2\omega_{\nu}}}\left(\frac{\partial\alpha_{\alpha\beta}}{\partial Q_{\nu}}\right)_0 \tag{12}$$

where $\alpha_{\alpha\beta}$ is the (complex) electronic polarizability. The CPP method provides a simple expression for RR scattering that is similar to the case of normal Raman scattering.[22] This approach is attractive not only due to its simplicity but also because it automatically handles near-degenerate excitations. One of its drawbacks, however, is its relatively large sensitivity to the phenomenological damping term that effectively accounts for the absorption band broadening.[18,23]

COMPUTATIONAL DETAILS

Our quantum chemical calculations of the ground-state equilibrium geometries, vibrational frequencies, and normal-mode analysis of the molecules in the gas phase were carried out with use of the Gaussian 03 program.[24] We employed the Gaussian 09 program[25] to describe, with a polarizable continuum approach, the ground and excited states of TNT and RDX in acetonitrile (ACN) solution to better mimic the experimental conditions of refs 5 and 6. RR spectra of the gas-phase molecules are calculated from vertical excitation energies and complex polarizabilities obtained from a locally modified version of the Dalton program,[26] based on the linear response solver recently presented in refs 27 and 28.

For the ground-state calculations, we adopted Kohn−Sham density functional theory (DFT), in conjunction with the B3LYP exchange-correlation (XC) functional and a triple-ζ cc-pVTZ basis set.[29] The basis set is sufficiently large so that no bias due to basis set incompleteness is expected. Vertical excitation energies are computed using time-dependent DFT (TDDFT) within the adiabatic approximation. In this case, we used the Coulomb attenuated B3LYP (CAM-B3LYP) functional[30] with parameters α = 0.19, β = 0.46, and μ = 0.33, in conjunction with the double augmented basis sets d-aug-cc-pVDZ.[29] The CAM-B3LYP functional, which is a hybrid long-range corrected functional, is expected to improve on the description of charge-transfer states, which are often significantly underestimated in TDDFT with standard local and semilocal XC functionals. To assess basis set errors, some of the excited-state calculations were repeated with the use of the d-aug-cc-pVTZ basis sets. These calculations of the absorption spectra did not significantly differ from the those done with the smaller basis sets. The effects of ACN on the ground- and excited-state properties of the equilibrium geometries were modeled using a polarizable continuum approach with ε = 2.38.[31]

The derivatives of the vertical excitation energies and polarizabilities of eqs 10 and 12 are carried out using a two-point numerical differentiation scheme. This is done by first performing a normal-mode analysis of the ground-state equilibrium structure, and then obtaining the mass-weighted normal coordinates Q by multiplying the eigenmodes by $1/M^{1/2}$ where M is the mass matrix. The finite displacements are then generated along Q with step lengths of $\pm 0.01 \times \mathrm{amu}^{1/2}$ where amu =1822.888 4843.

One drawback of the numerical approach for obtaining $\Delta_{e,\nu}$ is that the order of the excited states could change between different displaced geometries, which, if not treated carefully, would give errors in the numerical derivatives. Of course, this problem stems from the numerical differentiation used to compute the derivatives, and would thus be eliminated if analytical derivatives were used. In our calculations, since we used small displacements, this becomes an issue only for close-lying excited states. For the TNT conformers, the order of the first 15 excited states did not change between the displaced geometries as evidenced by the continuity of the excitation energies and the oscillator strengths. However, in two of the RDX conformers (AAE and AAA, see Figure 1), the excited states S_4 and S_5 are essentially degenerate and with nearly equal oscillator strengths. Numerical derivatives cannot in this case be evaluated straightforwardly to compute $\Delta_{e,4}$ and $\Delta_{e,5}$. Fortunately, in computing the RR spectra, we are concerned with the average over all excitations that are relatively close in energy, and, for these states, ambiguities in the numerical derivatives could be alleviated by adding up the corresponding $\Delta_{e,\nu}$ values. By inspecting eq 7, it is clear that this approximation becomes exact in the limit of identical oscillator strengths,

which is almost the case for S_4 and S_5 of the AEE and AAA RDX conformers (cf. Table 2).

The RR spectra using the VB and CPP approaches are computed using a locally developed code that takes as an input the vertical excitation energies and the polarizabilities of the displaced excited states along the mass-weighted normal coordinates Q. In the VB theory, the geometrical displacements $\Delta_{\epsilon,\nu}$ are first computed using eq 10, and then used in eq 9 to evaluate the Frank−Condon factors. The Raman polarizability tensor can then be computed after evaluating $\Phi(\omega)$ of eq 8 and using eq 7. A sufficient number of Franck−Condon factors were included in eq 8 to reproduce the main VB peaks of the spectrum, and for all cases the sum of the Franck−Condon factors is $\geq$0.9.

All of the theoretical approaches employed to study the RR spectra contain a phenomenological parameter to account for the finite lifetime of the excited states. The VB theory is not very sensitive to the value of the damping factor Γ in eq 8 in comparison to the other two approaches. For example, if we increase the value of Γ from 400 to 800 cm^{-1}, the Raman cross section for TNT would decrease by a factor of 3. The excited-state gradient and the CPP approaches are more sensitive to Γ.[18,23] In our calculations, we used a value of Γ = 400 cm^{-1} in calculations based on the VB theory and excited-state gradient approximation, and a value of Γ = 1000 cm^{-1} in the calculations based on the CPP approach.[32] In reporting spectra, the theoretical harmonic frequencies were scaled by a factor of 0.98 in order to account for anharmonicity effects and errors arising from use of the B3LYP functional.[33]

RESULTS AND DISCUSSION

Geometries. *TNT.* TNT has three nitro groups, two of which are out of plane with respect to the phenyl ring while the third one is planar. B3LYP calculations show that TNT has two low-energy conformers with C_s and C_1 symmetries that differ by an internal rotation of the methyl group.[34,35] Similar to previous studies,[35−37] we find that the C_s structure is lower in energy than the C_1 structure by 0.7 kcal/mol, mainly because the ortho-positioned NO_2 groups in the symmetric structure are rotated out-of-plane to reduce steric repulsion with the methyl group. Our value compares well with the results of 0.9 and 1.0 kcal/mol obtained previously at the DFT/B3LYP and MP2 levels of theory, respectively.[35] We investigated both TNT conformers since at room temperature both of them would contribute to the total population of TNT in the gas phase. For instance, given the computed B3LYP energy difference of 0.7 kcal/mol (including zero-point vibrational energies), the population of TNT would consist of 76% in the C_s structure and 24% in the C_1 structure, assuming a Boltzmann distribution with a degeneracy of one.

The structure and vibrational frequencies obtained in this study are in very good agreement with previous results. For example, the previous B3LYP/6-311+G(d,p) vibrational frequencies[35] are smaller than ours, but only by a few wavenumbers, with the exception of a small number of modes (7, 22, 24, and 31) that show 10−20 cm^{-1} discrepancies. Differences between the C_s and C_1 structures are also similar to that of previous studies.[35]

RDX. RDX is an important material used extensively in explosives. It has been investigated by several groups.[38−43] Different low-energy conformers were identified in the gas phase. RDX has three NO_2 groups bonded to nitrogen atoms of a triazine ring. Different RDX structures exist because the ring can occur as a chair, boat, or a twisted conformer. Additionally, conformers can differ by the arrangement of the nitro groups relative to the ring atoms. The naming scheme of the different structures indicates the axial (A) or pseudoequatorial (E) positioning of the nitro group with respect to the ring. Thus, the three nitro groups of the AAA (EEE) conformer occupy axial (pseudoequatorial) positions.

In the condensed phase, RDX has three polymorphs α, β, and γ.[38,40,44,45] The α-polymorph exists at ambient pressures and has orthorhombic structure where the eight molecules in the unit cell are all of the AAE type. The β-polymorph exists under high pressures and temperatures with RDX molecules belonging to the AAA type. Moreover, it is believed that the RDX molecule in the γ-polymorph, which is observed under high pressure, adopts the AEE conformation.

Rice and Chabalowski[38] performed geometry optimizations and normal-mode analysis of three conformers AAA, AAE, and EEA of RDX using the MP2 and DFT/B3LYP methods. They concluded that the AAA structure is the most probable conformer in the vapor-phase and β-solid RDX, and that crystal field effects are very small given the very similar crystal and optimized molecular geometries. In a later study, Vladimiroff and Rice showed using B3LYP that the barriers for the interconversion between the RDX conformers range between 1.5 and 5 kcal/mol, which suggests that measurements of RDX in the gas phase might reflect a dynamically averaged structure rather than a single dominant one.[40] The small energy difference between the conformers was also verified recently using a highly accurate correlated approach.[43] The geometries, harmonic frequencies, and excitation states of the six RDX conformers were optimized using MP2/6-311++G(d,p). Single-point energies were computed subsequently at the CCSD(T) level using these optimized geometries. At this level of theory, energy differences between the structures are between 0.2 and 5.2 kcal/mol.

We started from the six conformers of RDX (AAA, AAE, EEA, EEE, boat, and twist) that were identified previously[38,43] and optimized them at the B3LYP/cc-pVTZ level of theory. We find that the AAE isomer has the lowest energy, followed by the AAA, EEA, twist, and EEE conformers which are higher in energy by 0.4, 0.8, 0.9, and 3.9 kcal/mol, respectively. The boat configuration converged to the twist structure upon optimization. At the CCSD(T)/cc-pVTZ level with the molecular geometries optimized using MP2/6-311++G(d,p), the AAE is the lowest in energy, followed by the twist, AAA, EEA, boat, and EEE conformers which are higher in energy by 0.2, 1.2, 1.4, 2.1, and 5.2 kcal/mol, respectively.[43] The CCSD(T) values are reported without any basis set extrapolation and with use of the MP2 geometries; thus, the values cannot be accurate to within 1 kcal/mol as noted by the same study.[43] The zero-point vibrational energy corrections, as calculated using B3LYP/cc-pVTZ (in our case) and MP2/6-311++G(d,p) (results of ref 43), are considered in the ordering of the structures. Furthermore, we find in our calculations that all of the structures (except the boat conformer) to be minima on their respective potential energy surfaces with no imaginary frequencies. In the MP2/6-311++G(d,p) study,[43] the AAA and boat conformers are transition states with one imaginary frequency.

At any reasonable temperature the population of RDX in the gas phase will contain all of these low-lying energy conformers. For example, at T = 300 K, the Boltzmann population (assuming a degeneracy factor of 1) of RDX in the AAE, AAA,

Table 1. Vertical Singlet Excitation Energies E_{vert} (eV) and Oscillator Strengths (f) Contributing to the Lowest Electronic Absorption Band in the C_s and C_1 Conformers of TNT in the Gas Phase[a]

	C_s					C_1				
state	transition (wt)	E_{vert}	f	E_{vert}^{sol}	f^{sol}	transition (wt)	E_{vert}	f	E_{vert}^{sol}	f^{sol}
S_8	H−1 → L(77)	5.20	0.150	5.00	0.263	H−1 → L(55)	5.21	0.154	5.00	0.272
		(5.41)	(0.124)			H → L(20)				
		[5.22]	[0.148]							
S_9	H−1 → L+1(36)	5.58	0.217	5.36	0.293	H−1 → L+1(28)	5.57	0.180	5.35	0.275
	H → L(34)	(5.91)	(0.217)			H → L(21)				
		[5.63]	[0.226]							
S_{10}	H → L+1(41)	5.68	0.261	5.45	0.231	H → L+1(36)	5.69	0.211	5.48	0.200
		(6.00)	(0.374)							
		[5.72]	[0.306]							

[a]For each excitation, the largest contributing singly-excited configurations are shown with their corresponding percentage weights. Values in parentheses (brackets) are obtained using TD-LC-ωPBE (TD-LC-BLYP) as reproduced from ref 46.

EEA, twist, and EEE structures are 51%, 26%, 12%, 11% and 0.07%, respectively. Thus, we focus our study on the first four conformers.

Comparing with previous studies done at the B3LYP level of theory, our structural parameters and vibrational frequencies for the RDX conformers are in very good agreement with previous results.[38]

Excitation Energies and Absorption Spectra. *TNT.* Table 1 shows the vertical excitation energies E_{vert} and oscillator strengths of the three lowest excited states of TNT with appreciable oscillator strength. The dominant singly excited configurations are also shown. The vertical excitations and oscillator strengths obtained using TD-LC-BLYP and TD-LC-ωPBE are also reported.[46] Comparing the different TDDFT results, the CAM-B3LYP excitation energies and oscillator strengths of the C_s structure are in excellent agreement with TD-LC-BLYP values. However, they differ appreciably from the TD-LC-ωPBE results which show larger values of E_{vert}.

The UV absorption spectra of the two isomers of TNT are shown in Figure 2 from the CAM-B3LYP values. Also shown is the Boltzmann-averaged spectrum evaluated at T = 300 K. The two TNT conformers have similar absorption energies, at least for the first few excitations, despite the structural differences between them. The S_8 transition is separated from the pair of transitions S_9 and S_{10}.

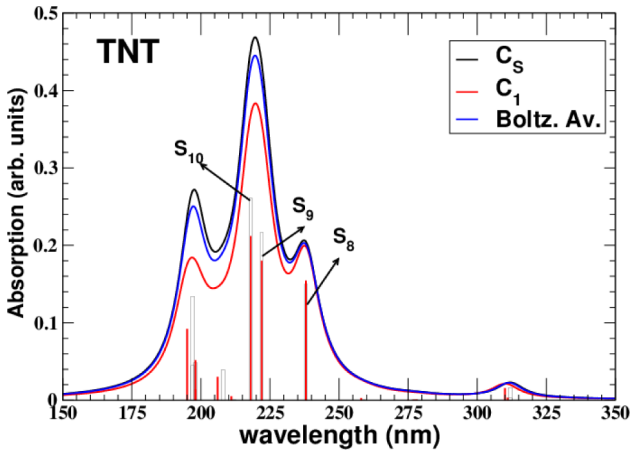

Figure 2. UV absorption spectrum of TNT in the gas phase as determined at the DFT/CAM-B3LYP level of theory. Oscillator strengths are indicated by vertical bars. The absorption band shape is obtained by the application of Lorentzian line broadening with a fwhm of 1000 cm^{-1}.

The UV absorption spectrum of the symmetric structure is in excellent agreement with previous results.[19] We also compared our results with the experimental spectra obtained for TNT in the gas phase[47] and in ACN.[5,6] In both cases, the experimental spectra are dominated by a broad structureless absorption peak with a maximum in the vicinity of 216 nm in the gas phase[47] and 229 nm in ACN solution.[5,6] This is reproduced in our calculations for the two TNT structures, where the absorption peak maximum is found at 219 nm, which is due to two separate intense transitions S_9 and S_{10} positioned at ≈222 and 218 nm, respectively, and with oscillator strengths of 0.22 and 0.26 for the C_s structure and 0.18 and 0.21 for the C_1 structure. S_9 is dominated by electron excitations from HOMO−1 to LUMO+1 and HOMO to LUMO while S_{10} is dominated by a transition from HOMO to LUMO+1. The shoulder of the absorption spectrum seen in the experimental spectra around 244 nm in the gas phase[47] and 266 nm in ACN solution[5,6] is also reproduced nicely at 244 nm in our calculations, and corresponds to the S_8 transition that is characterized by an electron excitation from HOMO−1 to LUMO. The frontier orbitals of the C_s TNT conformer that are involved in the S_8 and S_9/S_{10} excitations are shown in Figure 3.

Thus, the main features of the theoretical UV absorption spectrum of TNT are in excellent agreement with the experimental gas-phase results and those recorded in ACN solution. To quantify the effects of the solvent, we optimized the molecular structure of TNT in ACN solution with a continuum polarizable approach using B3LYP/cc-pVTZ, and then computed the vertical excitations using CAM-B3LYP/daug-cc-pVDZ. For convenience, we summarize the results in Table 1. As can be seen, solvent effects lead to red shifts in the S_8, S_9, and S_{10} energies of the C_s structure by 0.20, 0.21, and 0.23 eV, respectively. Similar shifts are observed for the C_1 isomer. The shifts in the S_9 and S_{10} energies bring them into excellent agreement with experiment with deviations less than 0.02 eV. Thus, we conclude that our results are in excellent agreement with measurements in the gas phase[47] or in ACN,[5,6] and that CAM-B3LYP and TD-LC-BLYP are describing well the absorption spectra of TNT, while TD-LC-ωPBE over-corrects the PBE excitation energy by ≈0.4 eV.

Furthermore, we note that solvent effects increase the oscillator strength of S_8 by almost a factor of 2 from 0.15 to 0.26, while it has less effect on the oscillator strengths of S_9 and S_{10}.

dx.doi.org/10.1021/jp303920c | J. Phys. Chem. A 2012, 116, 7862−7872

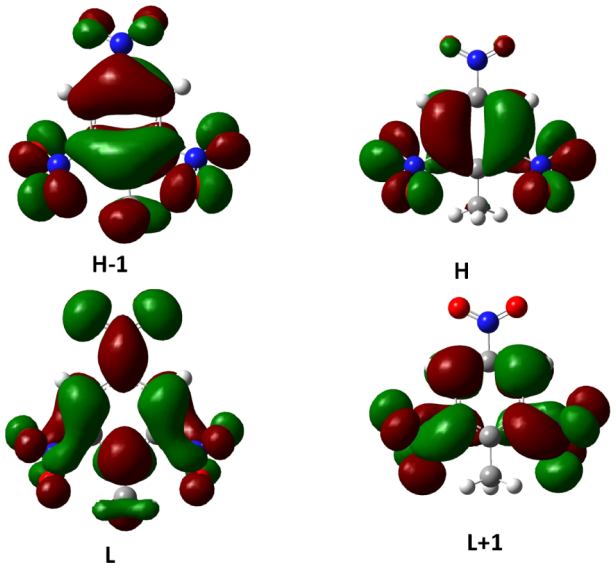

Figure 3. Frontier orbitals of C_s TNT conformer.

RDX. Table 2 presents the vertical excitation energies and oscillator strengths of the lowest four electronic excitations of the AAE, AAA, EEA, and twist conformers of RDX. The EEE conformer is not shown as its contribution to the RDX population is very small. For each excitation, the dominant excited configurations are also shown. For comparison, the excitation energies and oscillator strengths obtained recently using CCSD-EOM/6-311(2+,2+)G(d,p) are also reproduced in the table.[43]

Overall, there is very good agreement between the TDDFT and CCSD-EOM results, especially for the vertical excitations E_{vert} which indicates that the CAM-B3LYP exchange-correlation functional is well suited for describing the excited states of RDX. For the lowest energy isomer AAE, the difference between the TDDFT and CCSD-EOM E_{vert} values is less than 0.1 eV for the first three excitations. The oscillator strengths f differ somewhat between TDDFT and CCSD-EOM, but both methods agree on the ordering of the oscillator strengths with respect to the excitation level. For the AAA conformer, E_{vert} and f of S_4 and S_5 obtained with TDDFT compare favorably with the corresponding CCSD-EOM values. In both methods, these two excitations are degenerate or very close in energy, and with equal magnitude in their oscillator strengths. The TDDFT value for E_{vert} of S_6 shows a deviation of ≈0.5 eV with respect to the CCSD-EOM value, which is surprising considering the good agreement between the two sets of results. However, it is worth pointing out that the TDDFT value is in excellent agreement with the CIS value 5.52 eV.[43] EEA shows the best agreement between TDDFT and CCSD-EOM in both E_{vert} and f. Also, the lowest three excited states of the twist conformer compare favorably between TDDFT and CCSD-EOM.

A different perspective on the absorption data is given by relating it to the molecular structures illustrated in Figure 1. It appears reasonable to expect a near 3-fold degeneracy of states for the AAA and EEE conformers in which all nitro groups are nearly equivalent. This reasoning finds support in the DFT results presented in Table 2. First, we note that the AAE (EEA) conformer has two (one) state around 5.48−5.49 eV that we associate with axial arrangement of the nitro groups, whereas an equatorial arrangement is associated with a lower transition energy. Second, we note that the AAA and EEE conformer displays a near-3-fold degeneracy with transition energies of 5.53−5.55 and 5.44−5.48 eV, respectively, at the DFT/CAM-

Table 2. Vertical Singlet Excitation Energies E_{vert} (eV) and Oscillator Strengths (f) Contributing to the Lowest Electronic Absorption Band in the AAE, AAA, EEA, and Twist Conformers of RDX in the Gas Phase[a]

	AAE					AAA				
state	transition (wt)	E_{vert}	f	E^{sol}_{vert}	f^{sol}	transition (wt)	E_{vert}	f	E^{sol}_{vert}	f^{sol}
S_4	H−1 → L+1 (32)	5.41	0.014	5.49	0.060	H−10 → L(28)	5.53	0.020	5.54	0.076
	H−9 → L+1 (29)	[5.38]	[0.008]			H−3 → L+1(24)	[5.44]	[0.009]		
S_5	H−10 → L(35)	5.48	0.015	5.54	0.051	H−9 → L(28)	5.53	0.020	5.54	0.076
	H−2 → L+2(20)	[5.37]	[0.013]			H−3 → L+2(24)	[5.47]	[0.009]		
	H → L(16)									
S_6	H−10 → L+2(31)	5.49	0.013	5.61	0.049	H−3 → L(36)	5.55	0.008	5.61	0.017
	H−2 → L (27)	[5.39]	[0.007]			H−9 → L+2(26)	[6.09]	[0.008]		
	H−9 → L(15)					H−10 → L+1(19)				
S_7	H → L(66)	5.91	0.036	5.80	0.044	H−1 → L(48)	5.92	0.065	5.80	0.053
	EEA					twist				
state	transition (wt)	E_{vert}	f	E^{sol}_{vert}	f^{sol}	transition (wt)	E_{vert}	f	E^{sol}_{vert}	f^{sol}
S_4	H−10 → L(23)	5.44	0.012	5.54	0.077	H−9 → L(24)	5.47	0.003	5.55	0.087
	H−10 → L+1(21)	[5.45]	[0.010]			H−4 → L(21)	[5.39]	[0.003]		
	H−2 → L(16)					H−10 → L+1(19)				
	H−2 → L+1(16)									
S_5	H → L+2(16)	5.45	0.037	5.55	0.078	H−10 → L(33)	5.52	0.016	5.66	0.159
	H−9 → L (15)	[5.46]	[0.037]				[5.45]	[0.009]		
S_6	H−9 → L+2(27)	5.48	0.008	5.61	0.017	H−4 → L+2(44)	5.57	0.010	5.70	0.011
	H−1 → L+2(15)	[5.47]	[0.007]			H−9 → L+2 (30)	[5.53]	[0.006]		
S_7	H → L+2(36)	6.11	0.193	5.80	0.052	H → L(52)	5.78	0.110	5.74	0.022
		[6.24]	[0.229]				[6.01]	[0.083]		

[a]For each excitation, the largest contributing singly-excited configurations are shown with their corresponding percentage weights. Values in brackets are vertical excitation energies and oscillator strengths obtained at the CCSD-EOM/6-311(2+,2+)G(d,p) theory level as taken from ref 43.

dx.doi.org/10.1021/jp303920c | J. Phys. Chem. A 2012, 116, 7862−7872

B3LYP level of theory (and CCSD-EOM for EEE). In view of this systematicity, the coupled cluster result for the third state of the AAA conformer with a transition energy of 6.09 eV stands out as irregular and casts doubt upon its veracity. Most likely the CCSD-EOM converged into the higher excited state which is expected to have an excitation ≈6 eV.

It is interesting to note that the excitation energies of all of the conformers are very similar to each other despite the differences in their structures. In fact, this is also the case with the vibrational frequencies. Note, however, that the oscillator strengths show somewhat larger variations between conformers. Based on TDDFT and CCSD-EOM energies, the S_4, S_5, and S_6 excitations are all close in energy for all of the conformers, with differences less than 0.2 eV. Thus, it would be expected that all of these states would contribute to the RR spectrum for excitation that is in this energy range.

The UV absorption spectra of the four RDX conformers as well as the room temperature Boltzmann-averaged spectrum are shown in Figure 4. The spectra have broad absorption

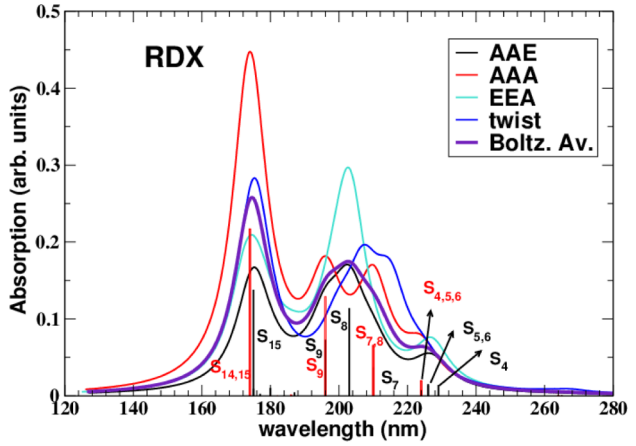

Figure 4. UV absorption spectrum of RDX in the gas phase as determined at the DFT/CAM-B3LYP level of theory. Oscillator strengths are indicated by vertical bars. The absorption band shape is obtained by the application of Lorentzian line broadening with a fwhm of 1000 cm^{-1}.

bands between 215 and 230 nm that are associated with the S_4, S_5, and S_6 excitations that have relatively similar oscillator strengths. The three bands would, thus, mimic a structureless flat band similar to that seen in the experimental absorption spectrum.[5]

The effects of the ACN solution are also investigated for the RDX conformers. For comparison purposes, we summarize our findings in Table 2. Compared to the gas-phase results, the ACN solvent leads to red shifts in the excitation energies for S_4, S_5, and S_6, and a blue shift for the S_7 excitation. Note, however, in contrast to TNT, these shifts are smaller in magnitude (less than 0.1 eV). On the other hand, the oscillator strengths of these excitations increase by factors as large as 5 (with the exception of S_5, where the oscillator strength is increased by a factor of 10). This is also opposite to the case of TNT. These changes in the oscillator strengths, and consequently $\boldsymbol{\mu}$, are very significant for the RR spectra because the intensity is proportional to $|\boldsymbol{\mu}^{eg}|^4$.

Resonance Raman Spectra. As a validity check for our program that is used to calculate the RR spectra, we have reproduced the recent results of Kane and Jensen on uracil[23] using the VB, excited-state gradient approximation, and CPP methods. In this investigation, we employed the same XC functional BP86[48,49] as in their study, but used instead Dunning's cc-pVTZ basis set that is of similar quality as the triple-ζ Slater basis set employed by Kane and Jensen. Our parametrization is very similar to theirs, as evidenced by the fact that the absorption wavelength for the second singlet state in uracil is equal to 265 nm which is in good agreement with their value of 262 nm. Our calculated Raman spectra (not shown) are also in very close agreement with the reported RR spectra,[23] and we conclude that our program has passed this validation criterion.

TNT. In Figure 5, we depict the RR spectra of the two TNT conformers. RR spectra obtained with use of the VB and

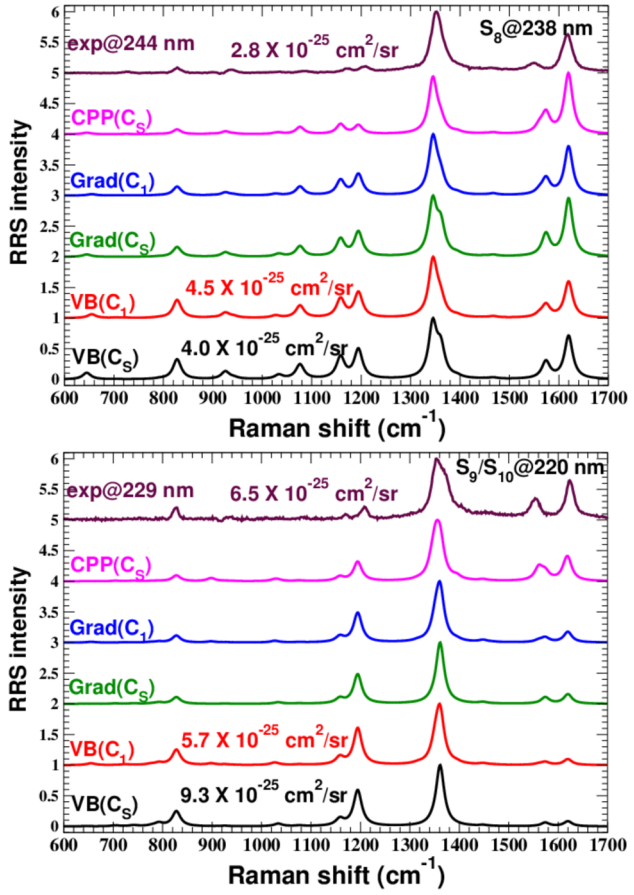

Figure 5. Resonance Raman spectra of the two TNT conformers. For the 220 nm excitation, we averaged over the S_9 and S_{10} excitations. The experimental spectra are from ref 6, and the maximum value of the Raman cross section is also shown. All spectra are scaled such that the maximum intensity is unity. The maximum value for the cross section is shown for the VB theory spectra where oscillator strengths are those of TNT in ACN solution for a better comparison with experiment. A Lorentzian broadening with a fwhm of 10 cm^{-1} was used.

excited-state gradient approximations are presented for both conformers whereas only the CPP approach was used for the symmetric one. We also show the experimental spectra of TNT in ACN solution.[6] All spectra are scaled such that the maximum intensity peak has unit intensity. To account partially for solvent effects and have a better comparison with experimental results, the maxima of the absolute Raman cross sections from

dx.doi.org/10.1021/jp303920c | J. Phys. Chem. A 2012, 116, 7862−7872

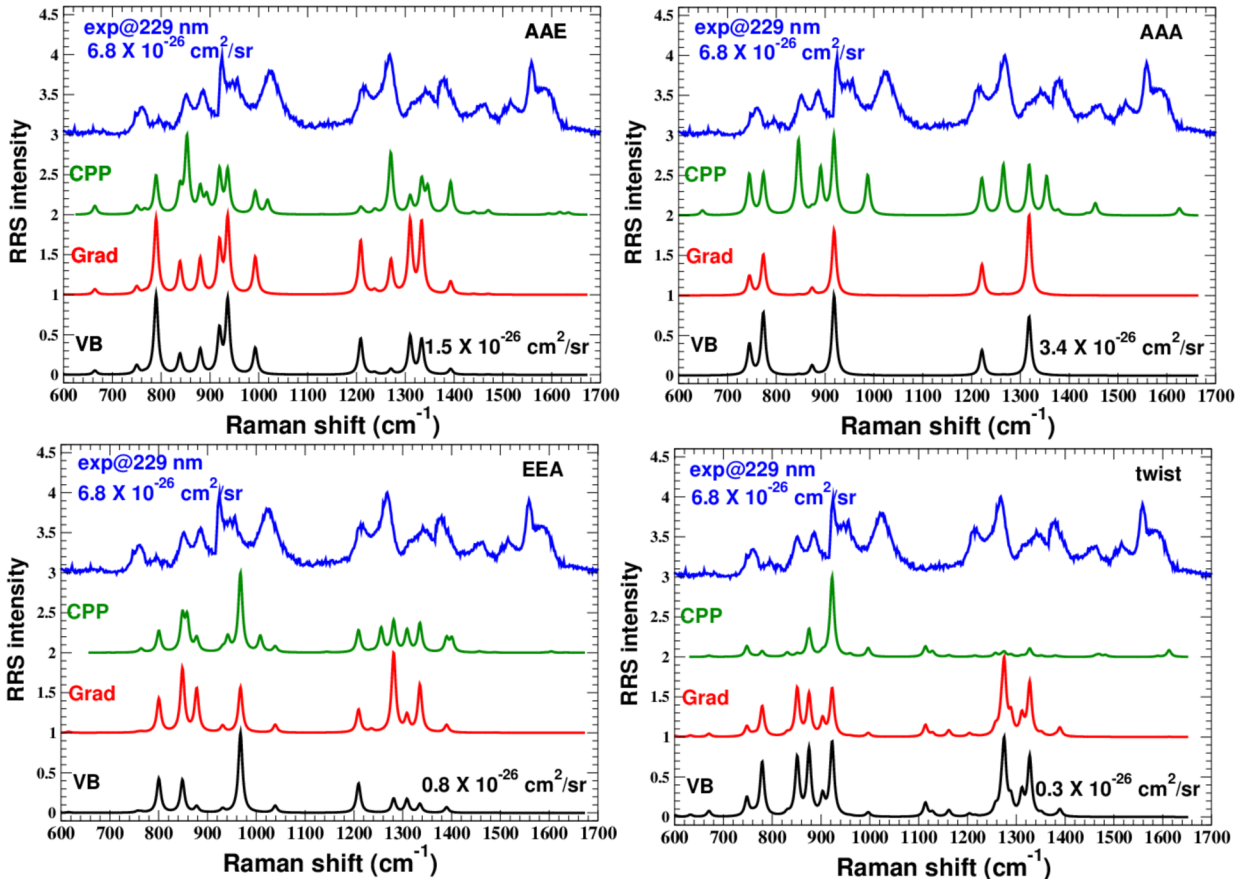

Figure 6. Resonance Raman spectra of RDX conformers. Otherwise, similar to Figure 5, except that in the VB theory and excited-state gradient approximation, we averaged over S_4, S_5, and S_6, while in the CPP method we used 226 nm excitation.

the VB theory are computed using the oscillator strengths of TNT in ACN.

On the basis of the frontier orbitals (shown in Figure 3 for the C_s conformer) that are involved in the S_8 and S_9/S_{10} excitations, we note that the most significant changes in the orbitals are associated with the NO_2 groups and the ring, and, thus, it would be expected that the vibrational modes that involve these atoms will be particularly enhanced. This explains why, for example, the ν_{40} mode around 1356 cm^{-1} which is associated with the symmetric stretching vibrational modes of NO_2 is particularly RR enhanced.

Despite the structural differences of the two conformers, the VB theory and excited-state gradient approximation results show that both spectra are very similar. The most notable differences occur for the strongly enhanced bands ν_{40}, ν_{41}, and ν_{42} with frequencies between 1344 and 1360 cm^{-1} that correspond to stretching modes of the NO_2 groups. In the symmetric structure, the ν_{40} and ν_{42} modes are both strong, while the ν_{41} mode is not active due to out-of-phase motions of the NO_2 groups. On the other hand, in the C_1 structure only the ν_{41} is strongly enhanced while the ν_{40} and ν_{42} modes are less enhanced. This explains the small shoulder in the spectra especially for the S_8 excitation. Additionally, these bands illustrate nicely why the RR spectra of the C_s structure have fewer features than those of the C_1 structure because of symmetry in the C_s structure (e.g., ν_{41} is not active).

The absolute Raman cross section of the most enhanced band at 1344 cm^{-1} in the C_s structure is 2-fold more intense than that in the C_1 structure for S_9/S_{10} excitation. However, its intensity is almost the same as that of the C_1 structure for S_8. By examining Table 1, we can see that these trends correlate with the oscillator strengths. Additionally, differences between the two RR spectra can be understood by examining the Kohn−Sham orbitals involved in the excitations. The S_8 transition is dominated by a transition from HUMO−1 to LUMO, where the electronic density of these two orbitals on the methyl group does not change much. This explains why the Raman cross sections for C_s and C_1 are rather similar since these structures differ mainly by an internal rotation of the methyl group.

Furthermore, it is reassuring that the three employed approaches for computing the RR spectra are in mutual agreement. Moreover, our CPP results for the S_8 excitation are in excellent agreement with the RR results presented by Mohammed et al.[19] for the S_8 excitation and which were obtained using a similar CPP approach.

The S_8 excited RR spectrum at 238 nm and S_9/S_{10} excitation at 220 nm RR spectra can be compared to the recently measured 244 and 229 nm spectra of TNT in ACN solution.[6] The S_8 excitation at 238 nm experimental spectrum shows a weak band around 826 cm^{-1}, a strong band around 1354 cm^{-1}, a weak band around 1550 cm^{-1}, and a semistrong band around 1600 cm^{-1}. The computed spectrum reproduces the experimental features showing the strongest band at 1345 cm^{-1} (ν_{40}) and the semistrong double-peak band at 1574 cm^{-1} (ν_{50}). Additionally, we see a semiweak band around 828 cm^{-1} (ν_{28}). Overall, the measured and calculated spectra also agree with the previously measured 238 nm RR spectrum of solid-phase TNT, although the peaks are somewhat shifted, perhaps due to crystal

dx.doi.org/10.1021/jp303920c | J. Phys. Chem. A 2012, 116, 7862−7872

constraints that are missing in TNT in the gas phase or solution.[50]

The locations of the peaks in the S_9/S_{10}@220 nm spectrum are also well reproduced. In particular, the RR spectrum shows a medium-weak band around 828 cm^{-1} (ν_{28}), a weak band around 1158 cm^{-1} (ν_{36}), and a medium weak band around 1200 cm^{-1} (ν_{38}). These are associated with the vibrational modes corresponding to the scissoring vibration of NO_2, CC-ring in-plane trigonal bending with C−N and C−CH_3 stretching, and a symmetric aromatic ring breathing mode, respectively. Additionally, the calculated spectra find that the strongest peaks occur at 1361 cm^{-1} (ν_{42}) that results mainly from the symmetric stretching vibrational modes of NO_2. The 1623 cm^{-1} experimental medium-strong bands show up as a medium intensity bands around 1619 cm^{-1} (ν_{52}) in our calculations.

Furthermore, we note that, in the experimental spectrum of TNT, there is a medium-strong band around 1554 cm^{-1} which is attributed to O_2 and not TNT.[5,6] In our calculations, a weak band appears in the spectrum around 1574 cm^{-1} (ν_{50}) for both structures of TNT that originates from NO_2 asymmetric stretching coupled to the ring. Thus, we conclude that the 1554 cm^{-1} band that is observed experimentally could also have a contribution from a TNT band. Overall, we find that the main enhancements for S_8, S_9, and S_{10} excitations occur for vibrations containing large components of the NO_2 stretching motions.

RDX. RDX is more challenging than TNT as it has at least four different conformers (with a 1 kcal/mol energy difference), all of which have somewhat similar vertical excitation energies but have larger differences in oscillator strengths (cf. Table 2). We show the calculated RR spectra of these conformers in Figure 6 for an excitation wavelength of 226 nm. Using the VB theory and excited-state gradient approximations, we averaged over the S_4, S_5, and S_6 excitations, as all conformers are within 0.1 eV. In the CPP approach, which can naturally handle nearby excitations, we used a single 226 nm excitation. For ease of comparison, we have scaled all spectra so that the maximum intensity peak has unit intensity. We show the maximum RR cross sections as calculated from VB theory, where the absorption oscillator strengths in this case are obtained from RDX in ACN.

In contrast to TNT, the RDX spectra show differences between the three different calculation methods. Overall, the VB theory and excited-state gradient spectra are in relatively good agreement, but these calculations differ from the CPP results. This shows that even though the excited-state gradient and CPP approaches are both based on the short-time approximation, they utilize different approximations. The near-degeneracy of the S_4, S_5, and S_6 excitations is a problem for the VB theory and the excited-state gradient approximation due to the ambiguity in computing the derivatives of the vertical excitations (we have remedied this to a large extent as discussed before). For comparison, the near-degeneracy of the excitations is not an issue in the CPP approach.

The RDX spectra of the different conformers show larger differences in Raman frequencies and relative intensities than those of the two TNT conformers. The spectra of the AAE and AAA conformers are in fact in better agreement than might appear at first glance. This is because the loss of symmetry in the AAE conformer compared to AAA causes a split of some of the bands in AAE that are degenerate in the AAA conformer. For example, the vibrational bands near 1320 and 930 cm^{-1} that are degenerate in the AAA conformer are split in the AAE conformer each into two bands.

Among the four RDX conformers, VB theory predicts that the AAE and AAA conformers have the largest RR intensities as can be seen from the values of the absolute RR cross sections in Figure 6. The VB theory RR spectra of AAE show two strong bands at 790 (ν_{24}, ring breathing plus NO_2 scissoring) and 936 (ν_{30}, C−N stretching plus CH_2-rock plus N−N stretching), and several semistrong bands around 839 (ν_{25}, N−N stretching plus NO_2 scissoring), 880 (ν_{27}, C−N stretching plus N−N stretching (axial)), 919 (ν_{29}, ring breathing), 993 (ν_{31}, N−N stretching (equatorial) plus CH_2-rock and CH_2-twist), 1209 (ν_{34}, CH_2-rock), 1310 (ν_{40}, CH_2-twist plus N−N stretching (axial)), and 1334 cm^{-1} (ν_{41}, CH_2-twist plus N−N stretching).

The AAA spectra from VB theory show three strong bands around 773 cm^{-1} (ν_{24}, N−N stretching in combination with O−N−O stretching and C−N stretching), 918 cm^{-1} (ν_{30}, ring breathing in combination with CH_2 scissoring and O−N−O stretching), and 1316 cm^{-1} (ν_{40}, N−NO_2 stretch and antisymmetric N−O_2 stretching). These are also strong or semistrong bands in the AAE conformers. The spectrum shows also three semistrong peaks around 745 cm^{-1} (ν_{21}, N−N stretching plus NO_2 scissor), 873 cm^{-1} (ν_{27}, C−N stretching + O−N−O stretching), and 1221 (ν_{34} cm^{-1}, CH_2-rock plus CH_2-scissor in combination with N−N stretch and ring breathing).

Examining the groups of atoms involved in the vibrational modes, we can infer which modes would be particularly RR enhanced. For example, the 1316 cm^{-1} (ν_{40}) band appears predominantly enhanced due to the large component of the N−NO_2 stretching where all of the N−NO_2 groups move in phase. In contrast, the similar ν_{38} and ν_{39} modes are not enhanced because the N−NO_2 groups move out of phase. The mainly methylene bending vibration modes (ν = 41−48) with frequencies between 1340 and 1420 cm^{-1} contain NN and NO_2 stretching that may yield some enhancement.

Given the small energy differences between the RDX conformers and also the small barriers that exist between them,[40] experimental Raman spectra of RDX obtained in the gas phase or in solution at finite temperatures would likely reflect a conformationally averaged structure, rather than a single dominant one.[40,43] This obviously complicates any direct comparison between the theoretical calculations and the experimental spectra of RDX in the gas phase or in solution. However, a better comparison of the computed spectra of the conformers would be with those obtained from high-quality single RDX crystals. Indeed, it is reported that the normal Raman spectra for the β and α RDX show significant differences.[42] Several distinct changes in the normal Raman spectra were also found between the α and γ phases.[45,51] We are not aware of any solid-state RR spectra of RDX in the condensed phase, so we compare our results with the recent experimental 229 nm RR spectra of RDX in ACN solution.[5,6]

Among the four RDX conformers, AAE and AAA would contribute the most to the RDX RR spectra in the gas phase or in solution. Comparing both sets of spectra with the measured spectra, there is some observable agreement, especially in the region of 700−1400 cm^{-1}. In clear contrast to the measured spectra, on the other hand, we note that all three theoretical methods yield spectra with only negligible RR scattering intensities in the 1400−1700 cm^{-1} region. The fact that all three methods agree in this prediction indicates that caution may be warranted in the interpretation of the experimental spectra. It is unlikely that these bands could derive from

photochemical degradation. Also, it is unlikely that the features are derived from overtones, which are not described with our formalism.

Finally, it is satisfying to see that the theoretical spectra are able to reproduce the order of magnitude difference in the absolute Raman cross sections of RDX compared to TNT observed experimentally. Also, from the differences that exist between the four RR spectra of RDX, it is clear that the particular arrangements of the three NO_2 groups make distinctive differences in the RR spectra. Thus, we would predict that HMX, which has four N−NO_2 groups, will show a significantly different RR spectra than RDX, as observed in the recent UVRR measurements.[5,6]

CONCLUSIONS

Using DFT methods, the UV absorption spectra and the UVRR intensities were calculated for TNT and RDX in the gas phase and for resonant excitations within the electronic absorption bands. The RR intensities are simulated using VB theory, excited gradient, and complex polarizability approaches. The latter two techniques are based on the short-time approximation. For TNT, all of the three methods agree with each other as well as with experimental results. Also, we show that the two TNT conformers have similar UV absorption and RR spectra. With 229 nm excitation, the absolute RR cross sections for the C_s conformer are twice those of the C_1 conformer, whereas they are of comparable magnitude with 244 nm excitation. The Kohn−Sham frontier orbitals show that vibrational modes that couple to the NO_2 and the ring electronic transitions are particularly resonance enhanced as verified in our computations.

For RDX, the four lowest energy conformers have somewhat different RR spectra. The AAE and AAA conformers have the largest RR scattering cross sections. A comparison with the experimental measurements in the gas phase or in solution is complicated because the RDX spectrum would result from a distribution of the conformations. Nevertheless, there are significant agreements between the computed RR spectra and UVRR experimental results. Similar to the TNT case, our results show that vibrational modes that couple to N−N or NO_2 are particularly enhanced. Moreover, for a 229 nm excitation, the computed RDX spectra show a 10-fold decrease in absolute Raman scattering cross sections compared to TNT cross sections which is also seen experimentally. Finally, the computed RDX RR spectra of the AAE, AAA, and AEE conformers predict the RR spectra of the α, β, and γ polymorphs of the solid phases of RDX.

AUTHOR INFORMATION

Corresponding Author

*E-mail: alsaidi@pitt.edu.

Notes

The authors declare no competing financial interest.

ACKNOWLEDGMENTS

W.A.S. thanks Nataliya Myshakina for many useful discussions at early stages of this work. Our calculations were performed in part at the University of Pittsburgh Center for Simulation and Modeling. P.N. acknowledges financial support from the Swedish Research Council (Grant No. 621-2010-5014) and a grant for computing time at National Supercomputer Centre (NSC), Sweden.

REFERENCES

(1) Asher, S. A. *Anal. Chem.* **1993**, *65*, 59A, 201A.
(2) Myers Kelley, A. *J. Phys. Chem. A* **2008**, *112*, 11975−11991.
(3) Oladepo, S. A.; Xiong, K.; Hong, Z.; Asher, S. A.; Handen, J.; Lednev, I. K. *Chem. Rev.* **2012**, *112*, 2604.
(4) Kiefer, W. *J. Raman. Spectrosc.* **2007**, *38*, 1538−1553.
(5) Tuschel, D. D.; Mikhonin, A. V.; Lemoff, B. E.; Asher, S. A. *Appl. Spectrosc.* **2010**, *64*, 425−432.
(6) Ghosh, M.; Wang, L.; Asher, S. A. *Appl. Spec.* **2012**, in press.
(7) Kramers, H.; Heisenberg, W. *Z. Phys. A Hadrons Nuclei* **1925**, *31*, 681−708.
(8) Dirac, P. A. M. *Proc. R. Soc. (London)* **1927**, *114*, 710.
(9) Albrecht, A. *J. Chem. Phys.* **1961**, *55*, 1476.
(10) Albrecht, A. *J. Chem. Phys.* **1971**, *55*, 4438.
(11) Heller, E. J. *J. Chem. Phys.* **1978**, *68*, 2066.
(12) Heller, E. J. *J. Chem. Phys.* **1978**, *68*, 3891.
(13) Lee, S.-Y.; Heller, E. J. *J. Chem. Phys.* **1979**, *71*, 4777.
(14) Peticolas, W. L.; Rush, T. *J. Comput. Chem.* **1995**, *16*, 1261−1270.
(15) Guthmuller, J.; Champagne, B. *J. Chem. Phys.* **2007**, *127*, 164507.
(16) Guthmuller, J.; Gonzalez, L. *Phys. Chem. Chem. Phys.* **2010**, *12*, 14812−14821.
(17) Guthmuller, J. *J. Chem. Theory Comput.* **2011**, *7*, 1082−1089.
(18) Jensen, L.; Zhao, L. L.; Autschbach, J.; Schatz, G. C. *J. Chem. Phys.* **2005**, *123*, 174110.
(19) Mohammed, A.; Agren, H.; Norman, P. *Phys. Chem. Chem. Phys.* **2009**, *11*, 4539−4548.
(20) Norman, P.; Bishop, D. M.; Jensen, H. J. Aa.; Oddershede, J. *J. Chem. Phys.* **2005**, *123*, 194103.
(21) Neugebauer, J.; Hess, B. A. *J. Chem. Phys.* **2004**, *120*, 11564−11577.
(22) Lee, S.-Y. *J. Chem. Phys.* **1983**, *78*, 723−734.
(23) Kane, K. A.; Jensen, L. *J. Phys. Chem. C* **2010**, *114*, 5540−5546.
(24) Frisch, M. J. et al. *Gaussian 03, Revision C.02*; Gaussian, Inc.: Wallingford, CT, 2004.
(25) Frisch, M. J. et al. *Gaussian 09 Revision A.1*; Gaussian Inc.: Wallingford, CT, 2009.
(26) DALTON, a molecular electronic structure program, Release 2.0 (2005); see http://www.kjemi.uio.no/software/dalton/dalton.html, 2005.
(27) Villaume, S.; Saue, T.; Norman, P. *J. Chem. Phys.* **2010**, *133*, 064105.
(28) Kauczor, J.; Jorgensen, P.; Norman, P. *J. Chem. Theory Comput.* **2011**, *7*, 1610.
(29) Dunning, T. H., Jr. *J. Chem. Phys.* **1989**, *90*, 1007.
(30) Yanai, T.; Tew, D. P.; Handy, N. C. *Chem. Phys. Lett.* **2004**, *393*, 51.
(31) Scalmani, G.; Frisch, M. J. *J. Chem. Phys.* **2010**, *132*, 114110.
(32) Norman, P.; Bishop, D. M.; Jensen, H. J. A.; Oddershede, J. *J. Chem. Phys.* **2001**, *115*, 10323−10334.
(33) Merrick, J. P.; Moran, D.; Radom, L. *J. Phys. Chem. A* **2007**, *111*, 11683−11700.
(34) Clarkson, J.; Smith, W. E.; Batchelder, D. N.; Smith, D. A.; Coats, A. M. *J. Mol. Struct.* **2003**, *648*, 203.
(35) Alzate, L. F.; Ramos, C. M.; Hern, N. M. *Vib. Spectrosc.* **2006**, *42*, 357−368.
(36) Golovina, N.; Titkov, A.; Raevskii, A.; Atovmyan, L. *J. Solid State Chem.* **1994**, *113*, 229−238.
(37) Janni, J.; Gilbert, B. D.; Field, R.; Steinfeld, J. I. *Spectrochim. Acta, Part A* **1997**, *53*, 1375−1381.
(38) Rice, B. M.; Chabalowski, C. F. *J. Phys. Chem. A* **1997**, *101*, 8720−8726.
(39) Harris, N. J.; Lammertsma, K. *J. Am. Chem. Soc.* **1997**, *119*, 6583−6589.
(40) Vladimiroff, T.; Rice, B. M. *J. Phys. Chem. A* **2002**, *106*, 10437.
(41) Byrd, E. F. C.; Scuseria, G. E.; Chabalowski, C. F. *J. Phys. Chem. B* **2004**, *108*, 13100−13106.

(42) Torres, P.; Mercado, L.; Cotte, I.; Hernandez, S. P.; Mina, N.; Santana, A.; Chamberlain, R. T.; Lareau, R.; Castro, M. E. *J. Phys. Chem. B* **2004**, *108*, 8799−8805.
(43) Molt, R. W.; Watson, T.; Lotrich, V. F.; Bartlett, R. J. *J. Phys. Chem. A* **2011**, *115*, 884−890.
(44) McCrone, W. C. *Anal. Chem.* **1950**, *22*, 954−955.
(45) Dreger, Z. A.; Gupta, Y. M. *J. Phys. Chem. B* **2007**, *111*, 3893−3903.
(46) Quenneville, J.; Greenfield, M.; Moore, D. S.; McGrane, S. D.; Scharff, R. J. *J. Phys. Chem. A* **2011**, *115*, 12286−12297.
(47) Usachev, A. D.; Miller, T. S.; Singh, J. P.; Yueh, F.-Y.; Jang, P.-R.; Monts, D. L. *Appl. Spectrosc.* **2001**, *55*, 125−129.
(48) Becke, A. D. *Phys. Rev. A* **1988**, *38*, 3098−3100.
(49) Perdew, J. P. *Phys. Rev. B* **1986**, *33*, 8822−8824.
(50) Munro, C. H.; Pajcini, V.; Asher, S. A. *Appl. Spectrosc.* **1997**, *51*, 1722−1729.
(51) Ciezak, J. A.; Jenkins, T. A.; Liu, Z.; Hemley, R. J. *J. Phys. Chem. A* **2007**, *111*, 59−63.